



Visible light photocatalytic activity of sol–gel Ni-doped TiO₂ on *p*-arsanilic acid degradation

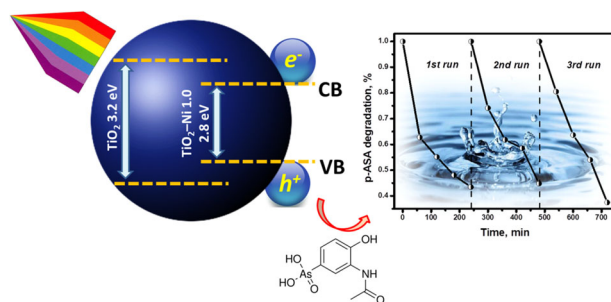
Mónica Patricia Blanco Vega¹ · Mariana Hinojosa-Reyes² · Aracely Hernández-Ramírez¹ · Jorge Luis Guzmán Mar¹ · Vicente Rodríguez-González³ · Laura Hinojosa-Reyes¹

Received: 3 September 2017 / Accepted: 6 January 2018 / Published online: 31 January 2018
© Springer Science+Business Media, LLC, part of Springer Nature 2018

Abstract

Nickel-doped TiO₂ (0.1, 0.5, 1.0, 2.5, 5.0, and 10.0 wt%) photocatalysts were prepared by the sol–gel method. Physicochemical properties were determined by the characterization using X-ray diffraction, Raman and UV–vis diffuse reflectance spectroscopies, N₂ physisorption, and zeta potential determination (PZC). The synthesized materials exhibited the photocatalytically active anatase crystalline phase and the catalysts exhibited stronger absorption in the visible light region with a red shift in the adsorption edge with the increase of Ni doping. The photocatalytic evaluation of TiO₂–Ni materials was carried out on *p*-arsanilic acid (*p*-ASA, 10 mg L⁻¹) degradation in aqueous suspension under visible radiation. Compared with bare TiO₂, the TiO₂–Ni 1.0 material (1 wt% Ni-doped TiO₂) exhibited higher photocatalytic activity on *p*-ASA degradation under visible light irradiation allowing a 76% degradation percentage in 180 min reaction time while 60% degradation percentage was achieved with undoped TiO₂. The TiO₂–Ni 1.0 material showed the highest surface area in comparison with the other prepared materials. Meanwhile, the photocatalytic activity of TiO₂–Ni 1.0 can keep even after three cycles with not loss of activity since nickel was not leached from the TiO₂-based catalyst into the solution during photocatalytic reaction. Therefore, the doping of the nickel into the TiO₂ lattice by the sol–gel method allowed its activation under visible radiation and an efficient photoexcited charge separation to prevent electron-hole recombination showing high chemical stability.

Graphical abstract



Keywords Nickel-doped-TiO₂ · *p*-arsanilic acid · Photocatalytic degradation · Visible radiation · Reusability · Stability

✉ Laura Hinojosa-Reyes
laura.hinojosary@uanl.edu.mx

¹ Universidad Autónoma de Nuevo León, UANL, Facultad de Ciencias Químicas, Cd. Universitaria, San Nicolás de los Garza, Nuevo León C.P. 66451, Mexico

² Universidad Autónoma de San Luis Potosí, Facultad de Ciencias, San Luis Potosí, SLP 78000, Mexico

³ Instituto Potosino de Investigación Científica y Tecnológica, IPICYT, División de Materiales Avanzados, Camino a la Presa San José 2055, Col. Lomas 4a. sección, San Luis Potosí, SLP 78216, Mexico

1 Introduction

Arsenic pollution has caused worldwide attention due to its mandatory toxicity. It has been linked to multiple health problems, including skin cancer, bladder cancer, diabetes, as well as cardiovascular diseases. Consequently, the U.S. Environmental Protection Agency listed arsenic as priority hazardous substance [1, 2]. Among arsenic compounds, the *p*-arsanilic acid (4-aminobenzenearsenic acid, *p*-ASA) is organoarsenic compound widely used in the poultry and swine industries as feed additive, that exhibits low metabolic rate in animals, i.e., 90% of the consumed mass is excreted unchanged [3, 4]. Land application of poultry manure is a common practice around the world due to high nutrient levels [4]. Consequently, it has been described elevated concentrations of arsenic in the pore water of agricultural soils after application of poultry manure [5, 6]. According to the World Health Organization guidelines for irrigation purpose the permissible limit of arsenic in water is 0.10 mg L^{-1} [2]. Thus, it is crucial to develop environmentally benign and more effective technologies for the removal of organoarsenic compounds from water to safe levels. In recent years, heterogeneous photocatalysis has been extensively applied on the oxidation of various refractory organic pollutants for environmental applications such as water and wastewater treatment [7, 8]. There have been few studies of the removal of organoarsenic compounds using TiO_2 -based photocatalysis [9–12], in contrast to the case for the oxidation of inorganic arsenic compound (As(III)) [1, 13–16].

So far, the TiO_2 has been the most studied semiconductor photocatalyst due to high photoactivity, low cost, low toxicity and good chemical and thermal stability [8]. TiO_2 catalyst can only be excited by UV light which only occupies a small part of the solar spectrum (~5% on earth) [17]. In order to improve the utilization of solar energy as an inexpensive and renewable energy source in photocatalytic applications, TiO_2 catalyst has been surface or structural modified with transition metal ions to extended its photoactivity into the visible range [7, 18]. The transition-metal impurities can be act as superficial potential traps of photo-generated electron-hole pairs. This process lengthen the lifetime of electrons and holes and increase the photoactivity [19]. Impregnation, co-precipitation, ion implantation technique, and sol–gel methods can be employed to incorporate transition metal ions dopants into TiO_2 [7]. The sol–gel method, a low-cost procedure, is the most commonly used soft wet-chemical method for the preparation of ordered mesoporous TiO_2 doped nanoparticles. The advantage of method is that facilitates the synthesis of nanometer sized crystallized TiO_2 powder of high purity at relatively low temperature. Additionally, this synthesis method shows high potential for controlling the bulk and

surface properties of the oxides and incorporation of dopant ions is performed on the molecular scale [7, 20].

Transition metal ion dopants as iron, cobalt, nickel, manganese, chromium, vanadium, copper, zinc, among others, have been investigated showing that have been able to modify the absorption spectrum of TiO_2 nanoparticles and extend its photocatalytic performance under visible radiation [8, 19]. Transition metal ions, specially nickel (Ni) has been demonstrated high potential as a dopant on TiO_2 due to the similar ionic radius of Ni^{2+} and Ti^{4+} ions (respectively 0.72 and 0.68 Å) and its inexpensive nature [21]. Ni^{2+} not only exhibits moderate toxicity, but it also possesses good chemical stability [22]. Ni-doped TiO_2 has been synthesized by various processing methods including sol–gel technique to increase photocatalytic activity of TiO_2 under UV, visible, and solar light radiation and have been mainly tested for degradation azo dyes [21, 23–28]; volatile organic compounds as xylene [29], toluene [30], and formaldehyde [31]; and phthalate esters [32].

In this work was evaluated for the first time the photocatalytic activity and its reusability under visible light of Ni-doped TiO_2 sample synthesized by sol–gel method on the degradation of *p*-arsanilic acid aqueous solution. The results showed that the prepared material is a promising photocatalyst to treat wastewater contaminated with environmentally harmful pollutants as organoarsenic compounds.

2 Experimental section

2.1 Catalyst synthesis

TiO_2 -Ni sol–gel photocatalysts were prepared by a sol–gel process using titanium (IV) isopropoxide (Sigma-Aldrich 97%) as titanium precursor and nickel nitrate hexahydrated (II) (97%, Sigma-Aldrich) as doped agent precursor; ethanol (Gpo. Le Cap 96%) and distilled water were used as solvents. Based on sol–gel processing route [33], the $\text{Ni}(\text{NO}_3)_2 \cdot 6\text{H}_2\text{O}$ solution (dissolved in water) was set at various weight percentages concentration (0.1, 0.5, 1.0, 2.5, 5.0, and 10.0 wt%) with respect to the titanium (IV) isopropoxide concentration to obtain Ni-doping. The TiO_2 -Ni catalyst was prepared by adding drop by drop 75.6 mL of titanium isopropoxide, 22.9 mL ethanol, 18 mL water and nickel solution to a 22.9 mL ethanol—18 mL water solution contained in a 4-neck round bottom flask (1 L) equipped with magnetic stirrer and thermometer. The molar ratio of alkoxide, ethanol and water was 1:3:8. Later on, the solution was vigorously stirred at 50 °C until all the reagents were added. In a subsequent step, the mixture was gradually heated to 70 °C. The gelled product was aged for 48 h at 70 °C. The solvents and unreacted precursors were removed

at 80 °C and dried overnight under vacuum at 100 °C. Finally, materials were thermally treated at 500 °C for 4 h at a heating rate of 2 °C min⁻¹. Samples were identified as TiO₂-Ni X, where X indicates the percentage of nickel (wt %). The bare TiO₂ catalyst was prepared according to the above procedure without the nickel (II) nitrate addition.

2.2 Catalyst characterization

The TiO₂-Ni X samples were characterized by X-ray diffraction (XRD) using a Bruker Advance 8 Diffractometer with CuK α radiation (1.5404 Å) with a step size of 0.02°. Rietveld refinement was carried out to determine the percentage of crystalline phase using the Maud software. The space group for anatase are (I41/amd); the atomic fraction coordinates are O²⁻ (0, 0.250, 0.166), Ti⁴⁺ (0, 0.250, 0.375); and the lattice parameters are $a = b = 3.785$ Å, $c = 9.520$ Å for anatase tetragonal. The space group for the rhombohedral NiTiO₃ was (R-3); the atomic fraction coordinates are Ni²⁺ (0.353, 0.353, 0.353), Ti⁴⁺ (0.142, 0.142, 0.142), O²⁻ (0.555, -0.055, 0.250); and the lattice parameters are $a = b = 5.032$ Å, $c = 13.792$ Å. Raman spectra were measured using a Micro-Raman Renishaw spectrometer equipped with an argon laser (633 nm). Diffuse reflectance UV-Vis using a DRUV-vis spectrophotometer Thermo Fisher Scientific-Evolution 300 equipped with a TFS-Praying Mantis integrating sphere. A sample of BaSO₄ (spectralon) was analyzed as reference. The band gap energy values of the materials were determined from their UV absorption spectra in the reflection mode. According to the Kubelka-Munk theory, the band gap was obtained by plotting $[F(R_{\infty}) \cdot E]^{1/2}$ vs. energy of the exciting light (E) assuming that materials showed direct allowed transition [34]. By extrapolating the linear part of the curve, the band gap energy transition can be derived. BET surface area was calculated from N₂ adsorption-desorption isotherm obtained in an Autosorb-1 instrument (Quantachrome Co., Boynton Beach, FL, USA). The point of zero charge (PZC) of TiO₂-Ni 1.0 catalyst was determined by potentiometric titration. Suspensions of catalyst were left in contact with 0.01 M KCl-0.004 M KOH solution. The mixture was stirred for 48 h to ensure a constant pH. Then, suspensions were titrated with 0.01 M HCl. The same procedure was used for blank solution (0.01 M KCl-0.004 M KOH). Equilibrium pH values were plotted as a function of acid volume added to obtain the potentiometric curves [35, 36]. The PZC was identified as the intersection point of the potentiometric curves with the blank.

2.3 Photocatalytic activity evaluation

The photocatalytic activity of pure and TiO₂-Ni powders was evaluated for *p*-ASA (99.0% purity, Sigma-Aldrich, St.

Louis, MO, USA) degradation reaction in an aqueous solution using a three high-intensity blue light LEDs lamp TRITAN™ 450 (450 nm, 358 watt m⁻², Spectroline) as a visible light source. In a typical experiment, 150 mL of 10 mg L⁻¹ aqueous *p*-ASA solution at desired pH was taken into glass reactor and the required amount of photocatalyst (catalyst loading of 0.50, 0.75, 1.00, 1.25, 1.50, and 1.75 g L⁻¹) was added and the suspension was magnetically stirred during 180 min. The solution pH was adjusted with 0.1 M HNO₃ or 0.1 M NH₄OH. Prior to photoreaction, the suspension was magnetically stirred in the dark for 60 min to establish absorption/desorption equilibrium condition. Under similar condition, an additional set of experiments were conducted (a) in the presence of catalyst (TiO₂-Ni but without visible power) to estimate the *p*-ASA removal by adsorption and (b) in the absence of catalyst and with visible power to estimate the *p*-ASA removal by photolysis. Aliquots of the reaction mixture were then withdrawn from the reactor at defined time intervals and filtered (0.45 μ m nylon syringe filter) before analysis. The aliquot sample was then analyzed by Perkin Elmer Series 200 HPLC using a Luna C18 250 \times 4.60 mm, 5 μ m reversed phase column (Phenomenex) and 1% acetic acid/methanol (97/3%, v/v) as mobile phase at a flow rate of 1 mL min⁻¹. The analyte was monitored at a wavelength of 250 nm. The chromatographic conditions were adapted from a previous work [37]. The total organic carbon (TOC) concentration during the degradation process was determined in the aqueous solution using a TOC-V CSH Shimadzu Analyzer. The chemical stability of the Ni doped TiO₂ catalyst was evaluated by reusing three times the photocatalytic material on *p*-ASA degradation under the same experimental conditions. In the last two cycles, the photocatalyst was separated by centrifugation, then washed with deionized water, and dried at 80 °C before the next test. The total nickel concentration, leached from the synthesized catalyst during its use was determined by the analysis of the water phase following the photocatalytic process by Atomic Absorption Spectrometry (AAS) (Varian SpectrAA 220 FS) using a PHOTRON hollow cathode nickel lamp using 232 nm emission line.

3 Results and discussion

3.1 Physicochemical properties

XRD characterization allowed the identification of crystalline phases of the photocatalysts. The diffractogram patterns are presented in Fig. 1. Anatase crystalline phase (JCPDS 04-002-2678) was only detected for photocatalyst with a low nickel content (0.0–1.0 wt%) whereas for materials with nickel contents higher (2.5, 5.0, and 10.0 wt%), nickel titanate (NiTiO₃) crystalline phase was also observed

(JCPDS 04-012-0745). In the Table 1 is shown the percentages of anatase and NiTiO₃ phases determined by Rietveld refinement method. The percentages of NiTiO₃ in TiO₂-Ni 2.5, TiO₂-Ni 5.0, and TiO₂-Ni 10.0 samples were 0.8, 4.6, and 20.9%, respectively. Thus, nickel ions in these materials exhibited tendency to segregate from the TiO₂ framework and crystallized as a NiTiO₃ phase. It has been described by Kakegawa et al. that anatase tetragonal and nickel titanate rhombohedral phases could coexist [38]. Table 1 summarizes the average crystallite size of anatase phase in the pure TiO₂ and TiO₂-Ni calculated by using the Debye–Scherrer formula. The crystallite size was found to be within the range 10.9–18.6 nm. Increasing nickel content from 0.1 to 5.0 wt% in the prepared catalysts decreased the crystallite size of the anatase phase in the samples showing restrained growth of TiO₂ crystals [39].

Raman spectra of the TiO₂-Ni photocatalysts are shown in Fig. 2. Raman vibrational modes occurred at frequencies

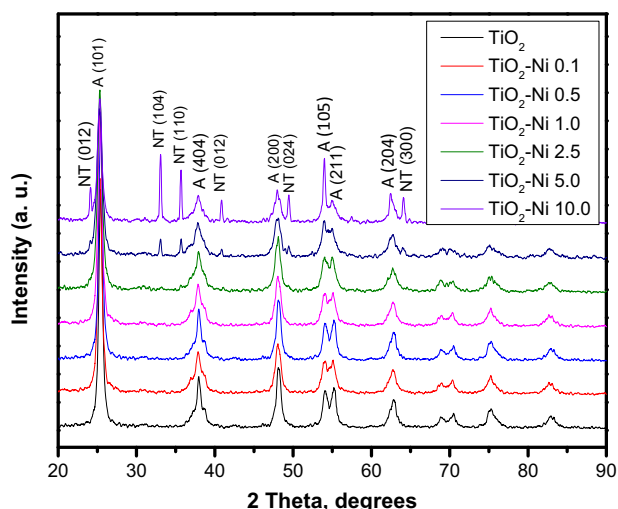


Fig. 1 XRD patterns of TiO₂-Ni photocatalysts, where A anatase, NT nickel titanate

of 144 (E_g), 199 (E_g), 399 (B_{1g}), 515 ($A_{1g} + B_{1g}$), and 640 (E_g) cm^{-1} corroborated the presence of anatase crystalline phase in these samples [40]. The E_g Raman vibrational mode at 141 cm^{-1} (Fig. 2a) of TiO₂-Ni samples showed an appreciable shift toward higher frequencies (from 143.2 to 145.0 cm^{-1}) by increasing the nickel content in the photocatalyst (see Fig. 2b). This E_g peak was assigned to the symmetric bending vibration of O–Ti–O in TiO₂ frame. The observed shift was attributed to the incorporation of Ni into the TiO₂ reducing the O/Ti ratio, suggested a shortening or rigidity of this chemical bond [41]. Six additional vibrational modes for the TiO₂-Ni, 10 photocatalyst were detected and tagged in the Fig. 2a. Those signals were attributed to the formation of NiTiO₃ crystalline phase [42] and were in agreement with XRD results.

Derived from the plot of the Kubelka–Munk function vs. energy (Fig. 3) were calculated the band gap energy (E_g) values shown in Table 1. The E_g values ranged from 3.2 to 2.0 eV. It was observed the reduction in the E_g value with increasing nickel concentration in the catalysts. This effect may be attributed to the Ni²⁺ doping into the TiO₂ lattice that creates extra energy levels situated within the bandgap of TiO₂. Therefore, the nickel incorporation promoted on TiO₂ lattice an extended absorption in the visible region [43].

An additional band was observed at 2.75 eV (450 nm, Fig. 3) for materials with NiTiO₃ crystalline phase TiO₂-Ni 5 and TiO₂-Ni 10. This band was due to the crystal field splitting of the 3d⁸ band associated with Ni²⁺ ions which splits up into two sub-bands called Ni²⁺ → Ti⁴⁺ charge transfer bands [44]. This result was supported by the NiTiO₃ crystalline phase segregation occurred for TiO₂-Ni materials with Ni content higher than 5 wt%.

The specific surface area (SSA) values determined for the Brunauer-Emmett-Teller method ranged from 57 to 95 $\text{m}^2 \text{g}^{-1}$ (see Table 1). While the content of the NiTiO₃ crystalline phase increased with the increasing of the nickel

Table 1 Detailed physicochemical properties of TiO₂-Ni photocatalysts

| | Crystalline phases ^a | Crystallite size ^b (nm) | E_g (eV) | λ_{max} (nm) | Specific surface area ($\text{m}^2 \text{g}^{-1}$) |
|---------------------------|--|---------------------------------------|------------|-----------------------------|---|
| TiO ₂ | A (100) | 16.3 | 3.2 | 387.5 | 86.6 |
| TiO ₂ -Ni 0.1 | A (100) | 18.6 | 3.2 | 388.7 | 72.7 |
| TiO ₂ -Ni 0.5 | A (100) | 16.6 | 3.2 | 393.6 | 81.0 |
| TiO ₂ -Ni 1.0 | A (100) | 13.9 | 2.8 | 436.6 | 95.4 |
| TiO ₂ -Ni 2.5 | A (99.2) ^c , NT (0.8) ^c | 13.3 | 2.9 | 427.5 | 90.8 |
| TiO ₂ -Ni 5.0 | A (95.4) ^c , NT (4.6) ^c | 10.9 | 2.6 | 476.9 | 77.8 |
| TiO ₂ -Ni 10.0 | A (79.1) ^c , NT (20.9) ^c | 13.7 | 2.0 | 629.4 | 56.9 |

^aA anatase, NT nickel titanate

^bCrystallite size of Anatase (101) crystallographic plane

^cPercentages of crystalline phases determined by Rietveld refinement

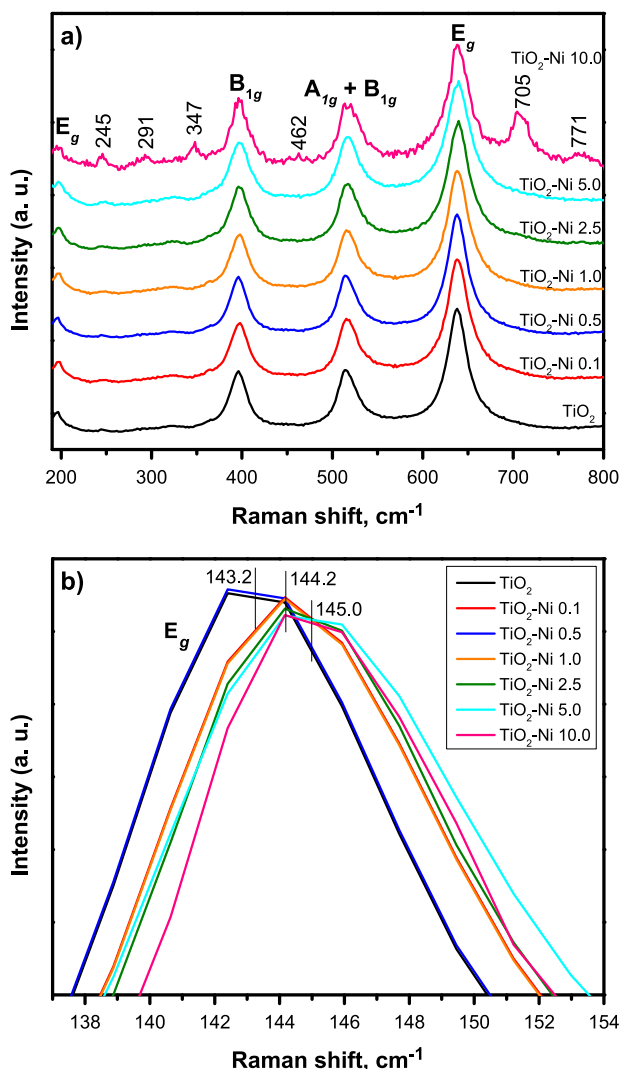


Fig. 2 Raman spectra of $\text{TiO}_2\text{-Ni}$ photocatalysts (a) vibrational modes of 195–800 cm^{-1} and (b) shift of the E_g vibrational mode (144 cm^{-1})

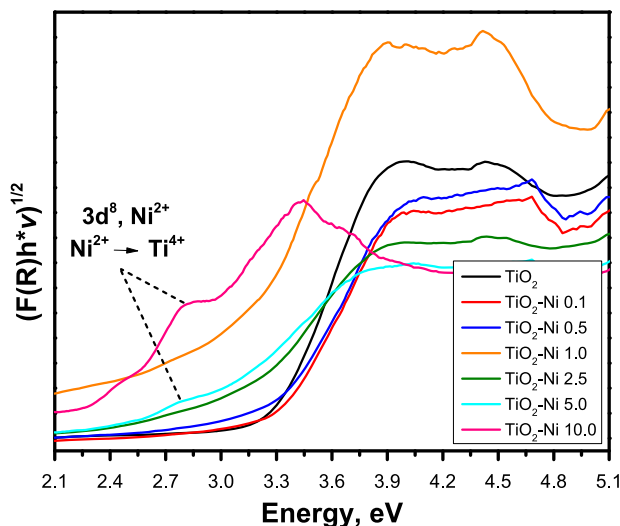


Fig. 3 Kubelka–Munk plot of $\text{TiO}_2\text{-Ni}$ photocatalysts

concentration the prepared catalysts, the SSA value decreased, showing the maximum surface area value ($95.6 \text{ m}^2 \text{ g}^{-1}$) for 1 wt% nickel doped TiO_2 material that presented only the anatase crystalline phase; higher nickel doping amount than 1 wt% in the TiO_2 lattice started to segregate as NiTiO_3 crystalline phase restricting the growth of the anatase crystalline phase [39, 44]. A photocatalytic material with high specific surface area provides abundant reactive sites for increasing the adsorption capacity of target organic pollutant molecules. The high surface area helps to improve the overall efficiency of the photocatalysis that occur at the interface of solid/liquid heterogeneous system due to the generation of higher amount of hydroxyl radicals, only if effective charge separation is achieved by the increased surface of $\text{TiO}_2\text{-Ni}$ photocatalyst [45, 46].

3.2 Photocatalytic activity of the $\text{TiO}_2\text{-Ni}$ photocatalysts

The pH of the *p*-ASA solution plays an important role in the photocatalytic degradation process. The degradation of 10 mg L^{-1} *p*-ASA solution was studied in pH range 3.0–9.0 using $\text{TiO}_2\text{-Ni}$ 1.0 (1 g L^{-1} catalyst loading) as photocatalyst under visible light irradiation. It was observed that the degradation percentage increases with increasing pH up to 5 and then slightly drops. The effect of pH on degradation percentage is shown in Fig. 4a. The $\text{pK}_{a1} = 2.7$, $\text{pK}_{a2} = 4.0$, and $\text{pK}_{a3} = 9.1$ [4] and the PZC of $\text{TiO}_2\text{-Ni}$ 1.0 experimentally determined by potentiometric titration was 6.54 ± 0.20 ($n = 3$). *p*-ASA exists as a cation below pK_{a1} , a neutral molecule between pK_{a1} and pK_{a2} , and an anion above pK_{a2} [4]. Thus, *p*-ASA is strongly adsorbed on the surface of catalyst under acidic conditions ($4.0 \leq \text{pH} \leq 6.54$) because of the electrostatic attraction of the negative charge associated with *p*-ASA and the positive charge associated with the $\text{TiO}_2\text{-Ni}$ 1.0. At $\text{pH} \geq 6.54$, *p*-ASA and $\text{TiO}_2\text{-Ni}$ 1.0 possess negative charges that will create electrostatic repulsion and reduce the level of surface adsorption.

It has been reported that catalyst loading affect photocatalytic efficiency for pollutant removal [7]. The effect of catalyst loading was also considered in the photodegradation of *p*-ASA at the optimum pH condition ($\text{pH} = 5$). Figure 4b shows an increased percentage of *p*-ASA degradation as the catalyst loading increased up to 1 g L^{-1} allowing a degradation percentage of 76.0% after 180 min of reaction. Degradation efficiency of *p*-ASA was not improved using catalyst loading higher than 1 g L^{-1} .

Results of *p*-ASA degradation under visible light irradiation in the presence of undoped TiO_2 and $\text{TiO}_2\text{-Ni}$ samples with different doping concentrations of Ni varying from 0.1 to 10 wt% are shown in Fig. 5a while the respective degradation rates are presented in Table 2. The

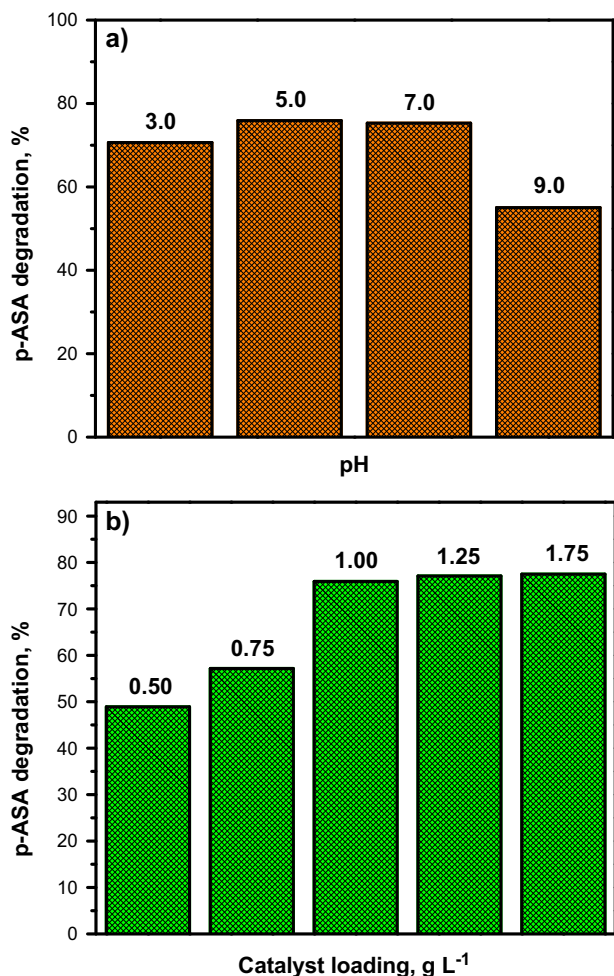


Fig. 4 Photocatalytic degradation of 10 mg L^{-1} p-ASA solution by $\text{TiO}_2\text{-Ni 1.0}$: (a) effect of pH using 1 g L^{-1} catalyst loading, and (b) effect of catalyst loading at pH = 5.0

photocatalytic degradation efficiency of $\text{TiO}_2\text{-Ni 1.0}$ was found to be better as compared to the other percentage of Ni doped TiO_2 samples and undoped TiO_2 . Specifically, the degradation percentages of p-ASA in 180 min reaction (after 60 min of dark adsorption–desorption equilibrium) were 43, 61, 76, 76, 62, and 42% degradation percentage for 0.1, 0.5, 1.0, 2.5, 5.0, and 10.0 wt% of Ni^{2+} doping, respectively while undoped TiO_2 showed 60% degradation percentage. Photocatalytic degradation of most organic pollutants at liquid–solid interface has been described by the Langmuir–Hinshelwood kinetic model and the degradation reaction rate can be expressed as *pseudo*-first-order model (Eq. 1) for low pollutant concentration [10, 21, 47].

$$-\log \frac{C_0}{C_t} = k_{app} t \quad (1)$$

where C_0 is the initial concentration of p-ASA (mg L^{-1}), C_t is t is the residual concentration of p-ASA at time (t) and k_{app} is the apparent rate constant (min^{-1}).

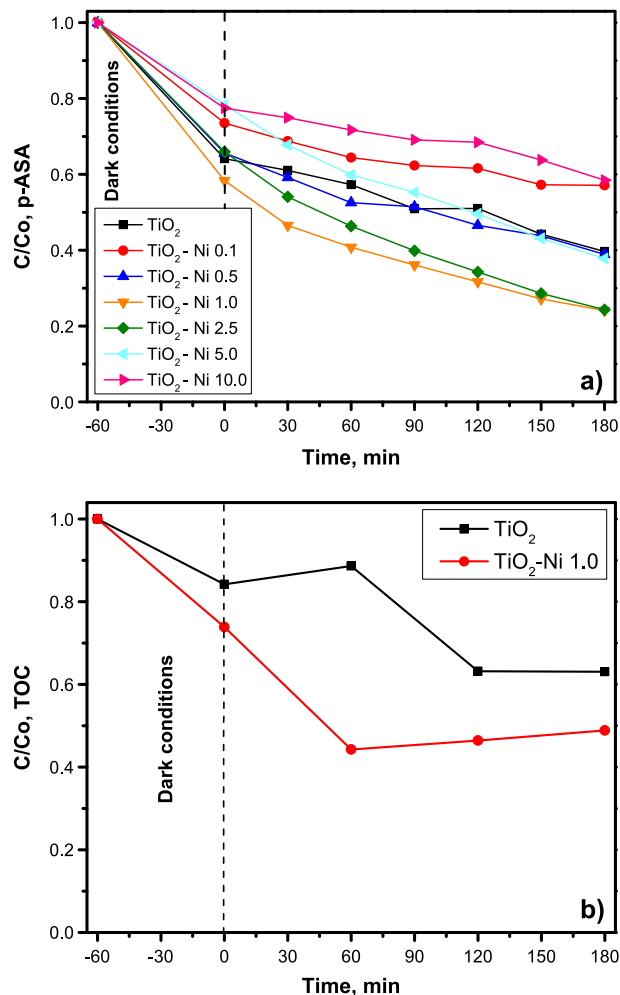


Fig. 5 Photocatalytic degradation of 10 mg L^{-1} p-ASA solution at pH = 5 using a catalyst loading 1 g L^{-1} under visible light: (a) the decrease in the p-ASA concentration (C/C_0) using various $\text{TiO}_2\text{-Ni}$ photocatalysts, and (b) comparison of mineralization (TOC) using $\text{TiO}_2\text{-Ni 1.0}$ and TiO_2 samples

Table 2 *Pseudo*-first-order kinetic parameters of the photocatalytic degradation of p-ASA for different $\text{TiO}_2\text{-Ni}$ photocatalysts

| Catalyst | $k_{app} \times 10^3 \text{ (min}^{-1}\text{)}$ | $t_{1/2} \text{ (min)}$ | R^2 |
|-------------------------------|---|-------------------------|--------|
| TiO_2 | 3.4 | 204.5 | 0.9279 |
| $\text{TiO}_2\text{-Ni 0.1}$ | 3.1 | 223.6 | 0.9205 |
| $\text{TiO}_2\text{-Ni 0.5}$ | 4.1 | 169.1 | 0.9225 |
| $\text{TiO}_2\text{-Ni 1.0}$ | 6.3 | 110.0 | 0.9620 |
| $\text{TiO}_2\text{-Ni 2.5}$ | 5.9 | 117.5 | 0.9927 |
| $\text{TiO}_2\text{-Ni 5.0}$ | 3.9 | 177.7 | 0.9939 |
| $\text{TiO}_2\text{-Ni 10.0}$ | 2.0 | 346.6 | 0.9261 |

The experimental data were observed to follow a *pseudo*-first-order kinetic. The correlation coefficients (R^2) > 0.9205, indicating reasonably good fit of the experimental data to the kinetic model. Although similar degradation percentages were achieved using $\text{TiO}_2\text{-Ni 1.0}$ and $\text{TiO}_2\text{-Ni}$

2.5 samples, reaction rate was higher for TiO₂-Ni 1.0 sample (Table 2).

The high photocatalytic activity of the TiO₂-Ni 1.0 catalyst can be attributed to its high surface area that enhances pollutant adsorption which influenced the subsequent photocatalytic activity. Additionally, the high photocatalytic performance TiO₂-Ni 1.0 was due to the optimum amount of dopant; larger amounts than 1.0 wt% nickel lead to an increase of intermediate states in the band gap, which inevitably act as recombination centers and thus decrease the photocatalytic efficiency of TiO₂ nanoparticles. At the optimal Ni doping amount, nickel can provide a shallow trap for photo-generated electron and hole so as to inhibit the recombination and extend the lifetime of charge carrier. Therefore, the photodegradation rate could be enhanced [23].

Photolysis and dark tests were performed as reference test to evaluate the contribution of light irradiation and/or adsorption to the degradation of *p*-ASA. The photolysis experiments during 180 min resulted in negligible degradation of *p*-ASA with less than 1% removal. On the other hand, the adsorption experiments (dark conditions) on TiO₂ Ni 1.0 catalyst demonstrated the higher adsorptive capacity of the *p*-ASA on the catalyst surface allowing 45.6% removal. According to the literature is well known that hydroxyl groups of the arsenic compounds can be strongly adsorbed with hydroxyl groups on the surface of TiO₂-based catalysts through interactions and bonding [9, 10, 48, 49]. The adsorption process of aromatic organoarsenic compounds as roxarsone and *p*-arsanilic acid on the TiO₂ surface was dominated by arsenate group via bidentate complexes [9].

Under optimal conditions, mineralization percentage of *p*-ASA solution under visible irradiation was 37% using TiO₂ while 51% of TOC abatement using TiO₂-Ni 1.0 sample was achieved (see Fig. 5b).

The photocatalytic activity of nickel doped TiO₂ materials with doping amounts of 0.5% prepared by liquid phase deposition technique [28] and 1.0% by coprecipitation and sol-gel dip coating techniques [21] have been tested under solar light for the degradation of standard dyes namely methylene blue and methyl orange, respectively allowing degradation percentages up to 100% in 180 min. The applicability of nickel doped TiO₂ materials synthesized by sol-gel method and polyol method has been evaluated for the oxidation of volatile organic compounds such as toluene and xylene vapors, [29, 30] under visible radiation where only was reached around of 45% degradation in 180 min reaction. Formaldehyde [31] and trichlorophenol [43] have also been tested as model pollutants through visible light photocatalytic degradation using this metal doped TiO₂ nanomaterial prepared by sol-gel technique, but have only degraded by around 5% after 180 min. By comparing the

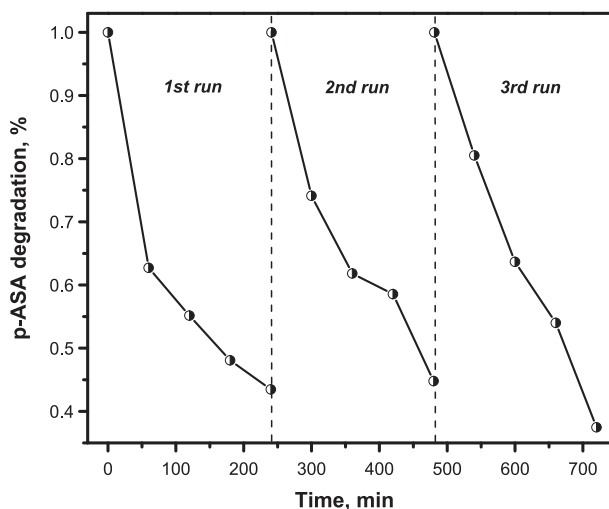


Fig. 6 Reuse of TiO₂-Ni 1.0 for the degradation of *p*-ASA under visible light irradiation. Reaction conditions: [*p*-ASA] = 10 mg L⁻¹, catalyst loading = 1.0 g L⁻¹ and solution pH = 5

above reports with our study, there have been no reports on photocatalytic degradation of compounds derived of arsenic using TiO₂-Ni 1.0 where near complete oxidation of *p*-ASA in pure water could be brought in the same reaction time therefore, according to our study the nickel doped TiO₂ materials represent an efficient and viable alternative to purify arsenic-contaminated wastewaters.

Besides photocatalytic activity, high stability is also important for photocatalytic nanomaterials in water remediation. The photocatalytic efficiency of the TiO₂-Ni 1.0 catalyst in three usages under visible light irradiation was confirmed to be similar under the same experimental conditions, as shown in Fig. 6. No obvious decrease in catalytic activity after three recycling tests indicated that the inherent structure of the TiO₂-Ni catalyst is stable toward continuous oxidative decomposition of the pollutant molecules. The stability of TiO₂-Ni 1.0 was also confirmed by measuring total Ni concentration in the solution after the first photocatalytic cycle by AAS technique (the method detection limit was found to be 0.01 mg L⁻¹). Negligible amount of leached Ni from the catalyst was detected in the solution indicating good chemical stability against corrosion of the TiO₂-Ni catalyst.

4 Conclusions

The photocatalytic degradation of *p*-ASA using nickel-doped TiO₂ materials prepared by sol-gel method under visible light irradiation was reported for the first time. Doping of Ni in TiO₂ promoted the formation of anatase phase, enhanced the surface area and reduced crystallite size. The sol-gel synthesis guaranteed the nickel

incorporation into the TiO₂ lattice that confers a red shift to light absorbing nature of TiO₂ and reduces its bandgap energy significantly so that it can absorb energy from a major portion of visible light; but also nickel-titanium photocatalysts acted as a mediator of interfacial charge transfer to suppress the electron-hole recombination.

During the photocatalytic degradation evaluation, the 1 wt% Ni doped TiO₂ material exhibited higher photocatalytic activity than bare TiO₂ in *p*-ASA degradation allowing 76% degradation percentage in 180 min reaction while undoped TiO₂ showed 60% degradation percentage. The strong binding of the nickel in the TiO₂ lattice allowed its reusability during three continuous cycles without loss of catalytic activity showing good chemical stability. Thus, these Ni doped TiO₂ materials could be applied during the photocatalytic degradation of other toxic arsenic species with the advantage of use the solar spectrum for its activation.

Acknowledgements The authors gratefully acknowledge financial support from PAICYT UANL and Facultad de Ciencias Químicas, UANL. We also thank the LINAN-IPICYT for the equipment and infrastructure provided. We wish to thank MC Beatriz Adriana Rivera Escoto and PhD Roberto Camposeco Solis for their valuable support.

Compliance with ethical standards

Conflict of interest The authors declare that they have no conflict of interest.

References

- Guzmán-Mar JL, Villanueva-Rodríguez M, Hinojosa-Reyes L (2015) Application of semiconductor photocatalytic materials for the removal of inorganic compounds from wastewater. In: Hernández-Ramírez A, Medina-Ramírez I (Eds.) Photocatalytic semiconductors: synthesis, characterization, and environmental applications. Springer International Publishing, Cham, pp 229–254
- Singh R, Singh S, Parihar P, Singh VP, Prasad SM (2015) Arsenic contamination, consequences and remediation techniques: a review. *Ecotoxicol Environ Saf* 112:247–270
- Mitchell W, Goldberg S, Al-Abadleh HA (2011) In situ ATR-FTIR and surface complexation modeling studies on the adsorption of dimethylarsinic acid and *p*-arsanilic acid on iron-(oxyhydr)oxides. *J Colloid Interface Sci* 358:534–540
- Mangalgi KP, Adak A, Blaney L (2015) Organoarsenicals in poultry litter: detection, fate, and toxicity. *Environ Int* 75C:68–80
- Chen WR, Huang CH (2012) Surface adsorption of organoarsenic roxarsone and arsanilic acid on iron and aluminum oxides. *J Hazard Mater* 227–228:378–385
- Zhu XD, Wang YJ, Liu C, Qin WX, Zhou DM (2014) Kinetics, intermediates and acute toxicity of arsanilic acid photolysis. *Chemosphere* 107:274–281
- Khaki MRD, Shafeeyan MS, Raman AAA, Daud W (2017) Application of doped photocatalysts for organic pollutant degradation—a review. *J Environ Manag* 198:78–94
- Pelaez M, Nolan NT, Pillai SC, Seery MK, Falaras P, Kontos AG, Dunlop PSM, Hamilton JWJ, Byrne JA, O’Shea K, Entezari MH, Dionysiou DD (2012) A review on the visible light active titanium dioxide photocatalysts for environmental applications. *Appl Catal B: Environ* 125:331–349
- Zheng S, Jiang W, Cai Y, Dionysiou DD, O’Shea KE (2014) Adsorption and photocatalytic degradation of aromatic organoarsenic compounds in TiO₂ suspension. *Catal Today* 224:83–88
- Zheng S, Cai Y, O’Shea KE (2010) TiO₂ photocatalytic degradation of phenylarsonic acid. *J Photochem Photobiol A Chem* 210:61–68
- Kim J, Kim J (2014) Arsenite oxidation-enhanced photocatalytic degradation of phenolic pollutants on platinumized TiO₂. *Environ Sci Technol* 48:13384–13391
- Lu D, Ji F, Wang F, Yuan S, Hu ZH, Chen T (2014) Adsorption and photocatalytic decomposition of roxarsone by TiO₂ and its mechanism. *Environ Sci Pollut Res Int* 21:8025–8035
- Zhang G, Sun M, Liu Y, Lang X, Liu L, Liu H, Qu J, Li J (2015) Visible-light induced photocatalytic activity of electrospun-TiO₂ in arsenic(III) oxidation. *ACS Appl Mater Interfaces* 7:511–518
- Garza-Arévalo JI, García-Montes I, Reyes MH, Guzmán-Mar JL, Rodríguez-González V, Reyes LH (2016) Fe doped TiO₂ photocatalyst for the removal of As(III) under visible radiation and its potential application on the treatment of As-contaminated groundwater. *Mater Res Bull* 73:145–152
- Guan X, Du J, Meng X, Sun Y, Sun B, Hu Q (2012) Application of titanium dioxide in arsenic removal from water: A review. *J Hazard Mater* 215–216:1–16
- Su H, Lv X, Zhang Z, Yu J, Wang T (2017) Arsenic removal from water by photocatalytic functional Fe₂O₃-TiO₂ porous ceramic. *J Porous Mater* 24:1227–1235
- Sang Y, Zhao Z, Zhao M, Hao P, Leng Y, Liu H, From (2015) UV to near-infrared, WS2 nanosheet: a novel photocatalyst for full solar light spectrum photodegradation. *Adv Mater* 27:363–369
- Di Paola A, García-López E, Ikeda S, Marci G, Ohtani B, Palmisano L (2002) Photocatalytic degradation of organic compounds in aqueous systems by transition metal doped polycrystalline TiO₂. *Catal Today* 75:87–93
- Daghrir R, Drogui P, Robert D (2013) Modified TiO₂ for environmental photocatalytic applications: a review. *Ind Eng Chem Res* 52:3581–3599
- Gupta S, Tripathi M (2012) A review on the synthesis of TiO₂ nanoparticles by solution route. *Open Chem* 10:279–294
- Ganesh I, Gupta AK, Kumar PP, Sekhar PS, Radha K, Padmanabham G, Sundararajan G (2012) Preparation and characterization of Ni-doped TiO₂ materials for photocurrent and photocatalytic applications. *Sci World J* 2012:127326
- Kumar RS, Dananjaya SHS, De Zoysa M, Yang M (2016) Enhanced antifungal activity of Ni-doped ZnO nanostructures under dark conditions. *RSC Adv* 6:108468–108476
- Gomathi Devi L, Kottam N, Girish Kumar S, Eraiah Rajashekhar K (2010) Preparation, characterization and enhanced photocatalytic activity of Ni²⁺ doped titania under solar light. *Open Chem* 8:142–148
- Chen C-Y, Hsu L-J (2015) Kinetic study of self-assembly of Ni (II)-doped TiO₂ nanocatalysts for the photodegradation of azo pollutants. *RSC Adv* 5:88266–88271
- Haque MM, Khan A, Umar K, Mir NA, Muneer M, Harada T, Matsumura M (2013) Synthesis, characterization and photocatalytic activity of visible light induced Ni-doped TiO₂. *Energy Environ Focus* 2:73–78
- Marathe SD, Shrivastava VS (2014) Photocatalytic removal of hazardous Ponceau S dye using nano structured Ni-doped TiO₂ thin film prepared by chemical method. *Appl Nanosci* 5:229–234
- Nakhate GG, Nikam VS, Kanade KG, Arbuñ S, Kale BB, Baeg JO (2010) Hydrothermally derived nanosized Ni-doped TiO₂: a visible light driven photocatalyst for methylene blue degradation. *Mater Chem Phys* 124:976–981

28. Begum NS, Farveez Ahmed HM, Gunashekar KR (2008) Effects of Ni doping on photocatalytic activity of TiO₂ thin films prepared by liquid phase deposition technique. *Bull Mater Sci* 31:747–751
29. Tseng H-H, Wei M-C, Hsiung S-F, Chiou C-W (2009) Degradation of xylene vapor over Ni-doped TiO₂ photocatalysts prepared by polyol-mediated synthesis. *Chem Eng J* 150:160–167
30. Khan R, Kim TJ (2009) Preparation and application of visible-light-responsive Ni-doped and SnO₂-coupled TiO₂ nanocomposite photocatalysts. *J Hazard Mater* 163:1179–1184
31. Zhang X, Liu Q (2008) Visible-light-induced degradation of formaldehyde over titania photocatalyst co-doped with nitrogen and nickel. *Appl Surf Sci* 254:4780–4785
32. Singla P, Pandey OP, Singh K (2015) Study of photocatalytic degradation of environmentally harmful phthalate esters using Ni-doped TiO₂ nanoparticles. *Int J Environ Sci Technol* 13:849–856
33. Hinojosa-Reyes M, Arriaga S, Diaz-Torres LA, Rodríguez-González V (2013) Gas-phase photocatalytic decomposition of ethylbenzene over perlite granules coated with indium doped TiO₂. *Chem Eng J* 224:106–113
34. López R, Gómez R (2011) Band-gap energy estimation from diffuse reflectance measurements on sol-gel and commercial TiO₂: a comparative study. *J Sol Gel Sci Technol* 61:1–7
35. Babić BM, Milonjić SK, Polovina MJ, Kaludierović BV (1999) Point of zero charge and intrinsic equilibrium constants of activated carbon cloth. *Carbon N Y* 37:477–481
36. Leyva Ramos R, Díaz Flores PE, Guerrero Coronado RM, Mendoza Barrón J (2004) A. Aragón Piña, Adsorción de Cd(II) en solución acuosa sobre diferentes tipos de fibras de carbón activado. *J Mex Chem Soc* 48:196–201
37. Chen D, Zhang H, Tao Y, Wang Y, Huang L, Liu Z, Pan Y, Peng D, Wang X, Dai M, Yuan Z (2011) Development of a high-performance liquid chromatography method for the simultaneous quantification of four organoarsenic compounds in the feeds of swine and chicken. *J Chromatogr B Anal Technol Biomed Life Sci* 879:716–720
38. Kakegawa K, Mohri J, Shirasaki S, Takahashi K (1982) Sluggish transition between tetragonal and rhombohedral phases of Pb(Zr, Ti)O₃ prepared by application of electric field. *J Am Ceram Soc* 65:515–519
39. Hinojosa-Reyes M, Zanella R, Maturano-Rojas V, Rodríguez-González V (2016) Gold-TiO₂-nickel catalysts for low temperature-driven CO oxidation reaction. *Appl Surf Sci* 368:224–232
40. Ohsaka T, Izumi F, Fujiki Y (1978) Raman spectrum of anatase TiO₂. *J Raman Spectrosc* 7:321–324
41. Zhu J, Ren J, Huo Y, Bian Z, Li H (2007) Nanocrystalline Fe/TiO₂ visible photocatalyst with a mesoporous structure prepared via a nonhydrolytic sol-gel route. *J Phys Chem C* 111:18965–18969
42. Lopes KP, Cavalcante LS, Simões AZ, Varela JA, Longo E, Leite ER (2009) NiTiO₃ powders obtained by polymeric precursor method: synthesis and characterization. *J Alloy Compd* 468:327–332
43. Zhao W, Ma W, Chen C, Zhao J, Shuai Z (2004) Efficient degradation of toxic organic pollutants with Ni₂O₃/TiO₂-xBx under visible irradiation. *J Am Chem Soc* 126:4782–4783
44. Lin Y-J, Chang Y-H, Yang W-D, Tsai B-S (2006) Synthesis and characterization of ilmenite NiTiO₃ and CoTiO₃ prepared by a modified Pechini method. *J Non Cryst Solids* 352:789–794
45. Khojasteh H, Salavati-Niasari M, Mortazavi-Derazkola S (2015) Synthesis, characterization and photocatalytic properties of nickel-doped TiO₂ and nickel titanate nanoparticles. *J Mater Sci Mater Electron* 27:3599–3607
46. Hyun Kim D, Sub Lee K, Kim Y-S, Chung Y-C, Kim S-J (2006) Photocatalytic activity of Ni 8 wt%-doped TiO₂ photocatalyst synthesized by mechanical alloying under visible light. *J Am Ceram Soc* 89:515–518
47. Kuo C-Y, Wu C-H, Lin H-Y (2010) Photocatalytic degradation of bisphenol A in a visible light/TiO₂ system. *Desalination* 256:37–42
48. Xu T, Cai Y, O'Shea KE (2007) Adsorption and photocatalyzed oxidation of methylated arsenic species in TiO₂ suspensions. *Environ Sci Technol* 41:5471–5477
49. Xu T, Kamat PV, Joshi S, Mebel AM, Cai Y, O'Shea KE (2007) Hydroxyl radical mediated degradation of phenylarsonic acid. *J Phys Chem A* 111:7819–7824